RSC Advances

PAPER

View Article Online
View Journal | View Issue

Cite this: *RSC Adv.*, 2014, **4**, 31230

Fabrication and electrochemical characterization of Zn–halloysite nanotubes composite coatings

S. Ranganatha and T. V. Venkatesha*

Zinc–halloysite nanotube (HNT) composite coatings through electrodeposition technique were successfully fabricated on mild steel substrate. As a comparison, pure zinc coating was also prepared. The composites were deposited in the presence of the surfactants cetyltriammonium bromide (CTAB) and sodium lauryl sulfate (SLS). The effect of the addition of nanoparticles and surfactants on the deposition, crystal structure, texture, surface morphology and electrochemical corrosion behavior were investigated. For the characterization of the electrodeposits, techniques such as X-ray diffraction (XRD) and scanning electron microscopy (SEM) coupled with energy dispersive X-ray analysis were used. Both the additives HNTs and surfactants polarize the reduction process and thus influence the deposition process, surface nature and electrochemical properties. Electrochemical experiments, such as potentiodynamic polarization and electrochemical impedance spectroscopy (EIS) studies, carried out in 3.5% NaCl solution show higher corrosion resistance by HNT incorporated coating, which was fabricated in the presence of CTAB. Microhardness of the deposits was evaluated and the composite with higher incorporation of nanoparticles in the presence of CTAB exhibited the highest value.

Received 1st April 2014
Accepted 23rd June 2014

DOI: 10.1039/c4ra02455a

www.rsc.org/advances

1 Introduction

Electrodeposition of zinc is a widely used industrial process for coating steel materials to enhance their service life. Zinc, being more active than iron, protects sacrificially by forming a white rust. This white rust can be controlled by chromating the surface of zinc using chromic acid. However, this is generally avoided as the chromating process produces effluents which pose environmental hazards. To overcome this limitation, some organic molecules were introduced as chelating agents and their thin films generated on zinc matrix with the idea of avoiding the interaction of corrosive medium with the metal matrix.[1] Increasing and demanding technological applications have led to the development of new coatings such as zinc alloy and/or zinc composite coatings. Metal/alloy coatings containing minute amounts of metal oxides, metal carbides, CNTs have been produced, which are called composite coatings.[2–6] Recent investigations on composite zinc coatings have revealed their higher corrosion resistance property with higher wear resistance and microhardness.[7–9]

Halloysite nanotubes (HNTs) are a type of naturally occurring aluminosilicate clay with a predominantly hollow nanotube structure. Halloysite is mainly composed of a two-layered aluminosilicate with the composition of $Al_2Si_2O_5(OH)_4 \cdot 2H_2O$, and is chemically similar to kaolinite, dickite or nacrite, differing mainly in crystal morphology. It is a layered clay mineral, consisting of one alumina octahedron sheet and one silica tetrahedron sheet in a 1 : 1 stoichiometric ratio. The lengths of HNTs vary in the range of 1–15 μm. HNTs have an inner diameter of 10–30 nm and an outer diameter of 50–70 nm, depending on the deposits. The chemical properties of the outermost surface of HNTs are similar to those of SiO_2, while the properties of the inner cylindrical core could be associated with those of Al_2O_3.[10]

Nanotubes with a hollow cavity have attracted a significant amount of interest in both scientific and industrial fields. They possess novel physical and chemical properties derived from structural versatility, and provide opportunities for advanced applications in the fields of electronics, optics, catalysis, energy storage, and biological systems. Carbon nanotubes of different kinds are being used for numerous applications. HNTs resemble CNTs from their unique crystal structure and are readily obtainable. Recent literature on HNTs has shown its potential as cheap alternatives to expensive CNTs because they possess tubular structure in nano-scale.[10,11]

The utility of HNTs is restricted to only some polymer composites, which results in higher and enhanced mechanical properties such as tensile strength, capacity to withstand force, *etc.* As far as corrosion is concerned, interestingly, these HNTs are utilized as nanocontainers for corrosion inhibiting organic molecules to achieve a regulated release of inhibitor. These HNTs have been successfully used in the fabrication of electroless Ni–P–HNT composite coatings, and showed improved properties of corrosion resistance, friction resistance and

Department of studies in chemistry, School of chemical sciences, Kuvempu University, Shankaraghatta-577451, Shimoga, Karnataka, India. E-mail: drtvvenkatesha@yahoo.co.uk; kamath.ranganath@gmail.com; Fax: +91-08282-256255; Tel: +91-9448855079

microhardness.[11] The success of a composite lies in the better reinforcement of secondary materials into the matrix. The use of surfactants of different structure and chemical nature to enhance particle density in coating and their effect on the process of electrodeposition has been reported previously.[7,8] Therefore, it will be of significant interest to study the HNT incorporated electrodeposits in the presence of different surfactants, which can impart new properties to surfaces.[12,13]

In this regard, HNTs with 50 nm diameter and several micrometers in length have been utilized for the development of surfaces and studies on changes in surface properties have been successfully carried out. In this work, HNTs have been incorporated into a growing zinc matrix. The effect of HNT inclusion has been studied by SEM, EDX and XRD. The surfactants cetyltriammonium bromide (CTAB) and sodium lauryl sulfate (SLS) have been used to improve the inclusion of particles. The corrosion studies have been carried out on the films through Tafel experiments and impedance spectroscopy. The results show that HNTs are novel composite materials that can improve corrosion stability in vigorous conditions.

2 Experimental

2.1 Materials

The composition of the plating bath for zinc and its composites is given in Table 1. The pH of the bath solution was 2.5 and it was adjusted by adding H_2SO_4. The halloysite nanotubes purchased from Sigma-Aldrich, product no. 685445, were used to fabricate the composite coatings. The agglomeration of nanotubes was minimized by subjecting the electrolyte to magnetic stirring for a period of 12 h and ultrasonication prior to the plating experiments.

The mild steel foils (AISI 1079 composition C = 0.5%, Mn = 0.5%, S = 0.005% and Fe = 98.95%) with dimensions of 40 mm × 40 mm × 1 mm was used as cathode substrate. A pure zinc (99.99%) anode with 40 mm × 40 mm × 1 mm dimensions was used for deposition. A potentiostat/galvanostat, model PS-618 (Chemilink systems, Mumbai), was used for the deposition of the coatings using DC currents. Throughout the composite deposition process, the electrolyte was stirred at a speed of 300 rpm. After electrodeposition, the samples were washed in distilled water for five minutes to remove the loosely adhering particles. Prior to plating experiments, the mild steel plates (cathode) were polished to smoothness using different grits of emery paper (600–4000) and degreased with trichloroethylene, followed by washing with water. The zinc (anode) surface was activated by dipping in 10% HCl for a few seconds, followed by washing with water.

Table 1 Composition of plating bath

Bath composition	Bath parameters
$ZnSO_4 \cdot 6H_2O$ – 200 g L^{-1}	pH – 2.5
Na_2SO_4 – 30 g L^{-1}	Current density – 5 A dm^{-2}
NaCl – 10 g L^{-1}	Duration – 10 min
CTAB – 0.2 g L^{-1}	
SLS – 0.2 g L^{-1}	
HNT – 1 g L^{-1}	

2.2 Characterization

2.2.1 Surface characterization. The surface morphology of the coatings was investigated using JEOL-JEM-1200-EX II scanning electron microscope. The particle content in the film was determined by energy dispersive X-ray analysis (EDX) coupled with SEM. X-ray diffraction (XRD) analysis of electrodeposits was carried out using a Philips TW 3710 X-ray diffractometer with Cu Kα radiation ($\lambda = 0.1540$ nm) operating at 30 mA and 40 kV.

2.2.2 FTIR studies. Fourier transform infrared spectra (FT-IR) were obtained on KBr pellets at ambient temperature using a Bruker FT-IR spectrometer (TENSOR 27).

2.3 Electrochemical studies

2.3.1 Cathodic polarization studies (deposition studies). For cathodic polarization studies, a disk of mild steel embedded in a Teflon holder with an exposed area of 0.13 cm^2 was used as a working electrode. Prior to each experiment, the mild steel electrode was first polished with different grits of emery paper (1200–4000), followed by alumina powders from 3 to 0.05 μm until a mirror finish was obtained. Cathodic scans were performed by ramping the potential from −0.4 V to −1.4 V. Electrochemical measurements were performed using a CHI660C electrochemical work station, and all of them were carried out at a temperature of 25 ± 2 °C. A conventional single compartment glass of three-electrode cell with 25 mL capacity, with a saturated calomel electrode as reference and a platinum wire as counter electrode was employed for the measurements.

2.3.2 Corrosion studies. Potentiodynamic polarization and electrochemical impedance spectroscopy measurements were performed using a CHI660C electrochemical work station. The measurements were performed using a conventional three-electrode cell, in which the test sample was placed in a Teflon sample holder, and the exposed surface area to the corrosive medium was approximately 1 cm^2. The platinum wire served as the counter electrode and the SCE electrode was the reference electrode. Prior to measurements, the sample was immersed in the corrosive medium (3.5% sodium chloride, pH neutral) to establish the open circuit potential (E_{OCP}) or the steady state potential. The potentiodynamic polarization measurements were performed at non-deaerated conditions.

2.3.2.1 Tafel studies. Tafel polarization study was used to calculate the kinetic parameters of the corrosion processes. The plots were obtained by varying the potential by ±200 mV from the open circuit potential at a scan rate of 0.01 V s^{-1} in 3.5% NaCl.

2.3.2.2 Electrochemical impedance spectroscopic studies. The electrochemical impedance spectrum was recorded in the frequency range of 10 mHz–100 kHz with a data density of 6 points per decade. After each experiment, the impedance data was displayed as Nyquist and Bode plots. The acquired data were curve fitted and analyzed using ZSimpWin 3.21 software.

2.4 Microhardness

The hardness of the coatings with a thickness of 15 μm was measured using Knoop's indenter (Clemex microhardness tester, made in Japan). The time of the application was 10 s with a load of 50 g. Microhardness values quoted are an average of 5 measurements performed at different locations on each coating.

3 Results and discussion

3.1 Characterization of HNTs: FTIR, SEM & TEM

The halloysite nanotubes utilized for the preparation of composite coatings were purchased from Sigma-Aldrich (product no. 685445). The SEM image in Fig. 1a shows the tubular structure of 1–3 μm long HNTs. As has been reported, HNTs contain two types of hydroxyl groups, inner and outer, which are situated between the layers and on the surface of the nanotubes, respectively. Because of the multi-layer structure, most of the hydroxyl groups are inner and only a few hydroxyl groups are located on the surface of HNTs. The surface of HNTs is mainly composed of O–Si–O groups, and the siloxane surface can be confirmed by Fourier transform infrared spectrum, Fig. 1b, in which a very strong absorption of O–Si–O at around 1020 cm^{-1} is observed. The 1094 cm^{-1} peak is assigned for the stretching mode of apical Si–O. Two Al_2OH stretching absorptions at 3618 and 3695 cm^{-1} were observed. Si–O bending absorbs at 462 cm^{-1} and a single Al–OH bending at 918 cm^{-1}.

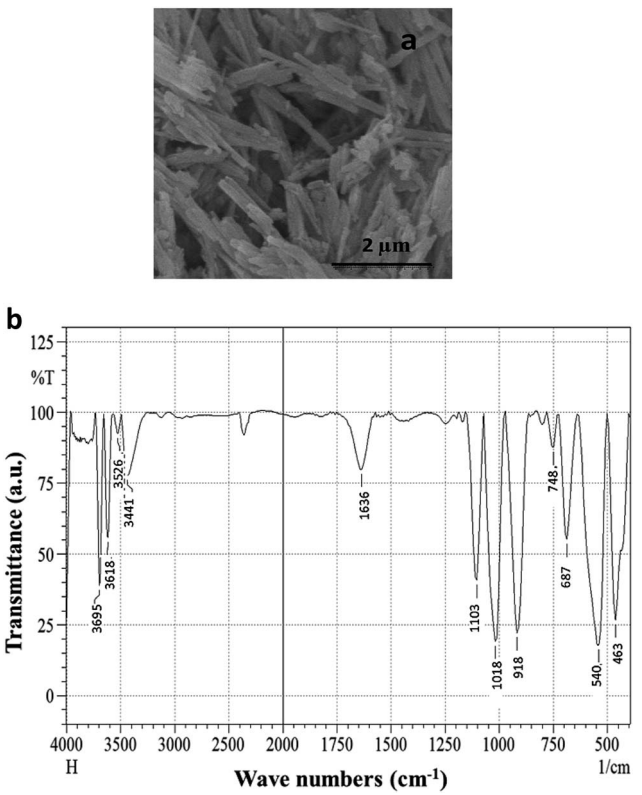

Fig. 1 (a) SEM image of halloysite nanotubes. (b) FTIR spectrum of HNT.

The band observed at 540 cm^{-1} is of the deformation vibration of Al–O–Si. The absorption at 3441 cm^{-1} is attributed to O–H stretching of water and that of 1636 cm^{-1} to O–H deformation of water. The peaks at 687 and 748 cm^{-1} are assigned to the perpendicular Si–O stretching.[14,15]

3.2 Coating characterization

The Fig. 2a shows the surface morphology of the zinc electrodeposits of 15 μm thickness. The image C_0 shows zinc deposit without any additives. C_C, which is a HNT composite of zinc metal, shows a modified surface compared to the plain zinc. The HNT particles change morphology, forming smaller crystallites. The C_{CC} and C_{CS} represent the Zn–HNT composites in the presence of the surfactants CTAB and SLS. It can be easily identified that the morphology of the composite fabricated with CTAB is severely modified compared to that of the composite prepared with SLS. Additives increase nuclear number, thereby creating competition between nucleation and crystal growth. During the electrodeposition process, metal ions from the electrolyte reduce onto the surface of the cathode. The additives that were carried along with the metal ions towards the cathode cover the reduced metal nuclei, facilitating the formation of newer nuclear sites. This phenomenon prevents crystal growth on a particular metal seed, which is most beneficial to attain fine grained morphology, because it provides a larger number of nuclear sites on the deposit. In the case of CTAB, the development of a positive charge on the surface of the particles is expected because of which more particles drift towards the cathode, leading to larger incorporation that ultimately results in finer grained crystal structure of the coating compared to other coatings. Further, EDX results presented in the next segment reflect the influence of surfactants on the amount of particle reinforcement to the coating. Thus, the introduction of particles and surfactant molecules result in smaller grain sizes. Fig. 2b shows the cross sectional SEM images of zinc and zinc composite. C_{CC} clearly shows the incorporated particles in the presence of CTAB.

The coating composition was evaluated by the EDX technique. Fig. 2c shows the EDX spectra for Zn and Zn–HNT composite, and Table 2 presents the elemental composition of the deposits. Different kinds of surfactants were used and their effect on the incorporation of particle into the metal matrix, reduction process and surface nature has been investigated. For this purpose, a cationic surfactant CTAB and an anionic surfactant SLS were used. A certain amount of surfactant was added to the electrolytic bath containing particles under mechanical stirring. EDX analysis shows that HNT incorporation is of around 3.7 wt% in deposit C_C, and varies with the addition of surfactants. CTAB increases its incorporation to 4.8 wt%, whereas SLS to 4.1 wt%. The surfactants aid the ease of particle incorporation by facilitating good dispersion in the electrolyte. However, CTAB shows a higher performance in increasing particle incorporation by creating a positive charge on the particle surface because it is a cationic surfactant. The positive charge attracts the particles towards the cathode.

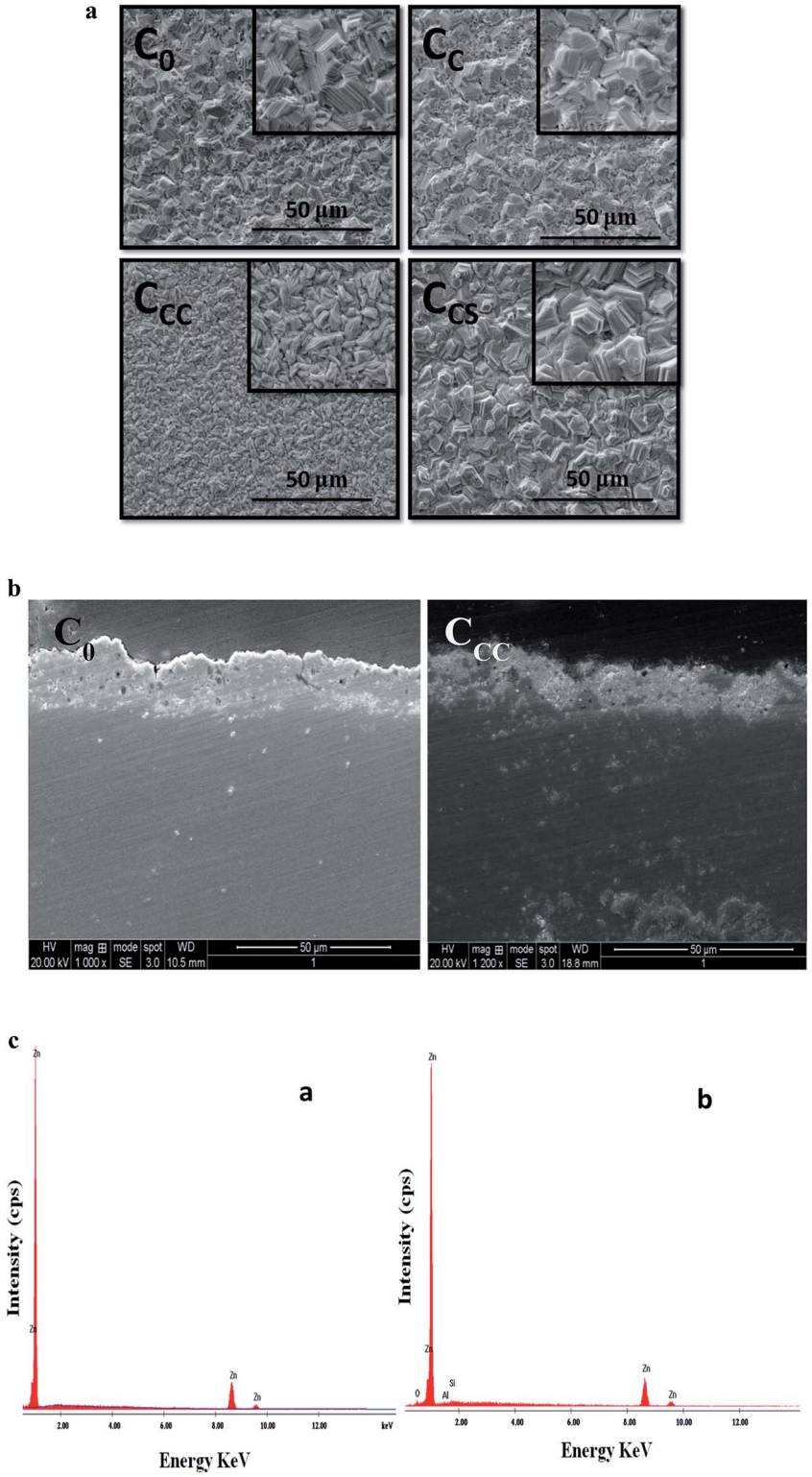

Fig. 2 (a) SEM images of the zinc and zinc composite coatings in different conditions. (b) SEM cross sectional images of zinc and zinc–HNT composite. (c) EDX spectra of (a) zinc and (b) Zn–HNT composite coating.

Fig. 3 displays the X-ray diffractograms and texture coefficients obtained for zinc deposits. It signifies the effect of surfactants and nanoparticles on the crystallographic orientation and crystallinity of the deposits.

The determination of the textures of the deposits is of considerable interest because the electrocrystallization of zinc is very sensitive to bath composition. The preferred orientations

Table 2 Elemental composition of the deposits obtained from EDX analysis

Sample	Elemental composition in wt% Zn	HNT
C_0	100	—
C_C	96.3	3.7
C_{CC}	95.2	4.8
C_{CS}	95.9	4.1

of the deposits were determined using Muresan's method calculating the texture coefficients (T_c) using equation [2]

$$T_c = \frac{I_{(hkl)}}{\sum I_{(hkl)}} \times \frac{\sum I_{0(hkl)}}{I_{0(hkl)}}$$

where $I_{(hkl)}$ is the peak intensity of the zinc deposits and ΣI is the sum of the intensities of the independent peaks. The index '0' refers to the intensity of a standard zinc powder sample. The preferred crystallographic orientation is indicated by a T_c value larger than unity. The development of different crystal structures can be related to surface energy differences that become the driving force for the relative growth of grain, which have the lowest surface energy; (0 0 2) plane has the lowest surface free energy due to its compactness. The zinc coating except C_{CC} preferentially orients in the (0 0 2) plane, indicating the effect of CTAB on crystal structure. The majority of Zn crystallites in pure zinc coating are oriented parallel to (1 1 0), (1 0 2) and (0 0 4) planes. The inclusion of the particles orients the zinc crystallites along (0 0 2) and (0 0 4) to a large extent. The surface morphologies of the deposits in the presence of surfactants have been modified, CTAB is sufficiently strong to change the crystal structure in comparison with SLS. The most intense peak in the presence of CTAB is (1 0 1). The marked decrease in the basal (0 0 2) plane intensity is because of the modification of the surface energy of the metal by the adsorption of organic molecules. Increased surface energy is also responsible for the deviation of hexagonal crystal structure with the addition of CTAB. The addition of particles and SLS does not have much effect on the crystallographic orientation.[16,17]

3.3 Deposition studies: cathodic polarization

Fig. 4 shows the cathodic polarization curves of the Zn–HNTs with and without the surfactants. The deposition studies illustrate that HNTs have an obstructive effect on Zn^{2+} reduction. In literature, it has been reported that the metal Me^{2+} occurs in several steps. It is accepted that an intermediate Me^{+} adsorption on the electrode occurs during the cathode reaction.[1,18] During this, the localized concentration of hydroxide ions in close proximity to the cathode surface will increase and result in the formation of $MeOH_{ads}$. The probable chemical reaction path of the reduction of zinc ions is specified below.[19]

$$Zn^{2+} + H_2O \rightarrow (ZnOH)^{2+} + H^+$$

$$(ZnOH)^{2+} + e^- \rightarrow Zn(OH)_{ads}$$

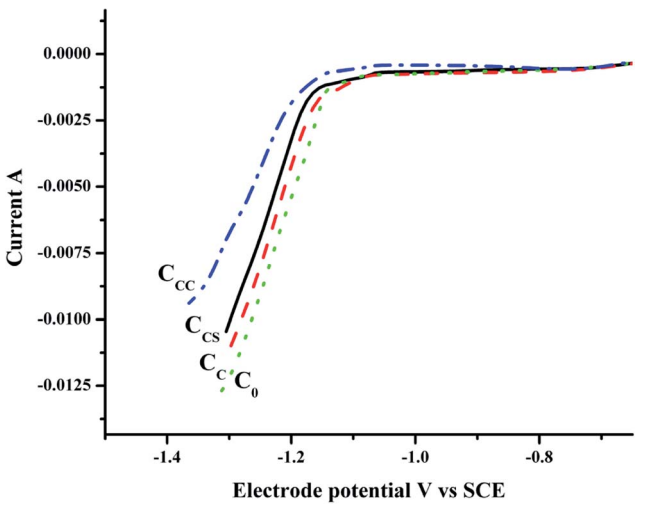

Fig. 4 Cathodic polarization curves for composite bath solutions with and without surfactants.

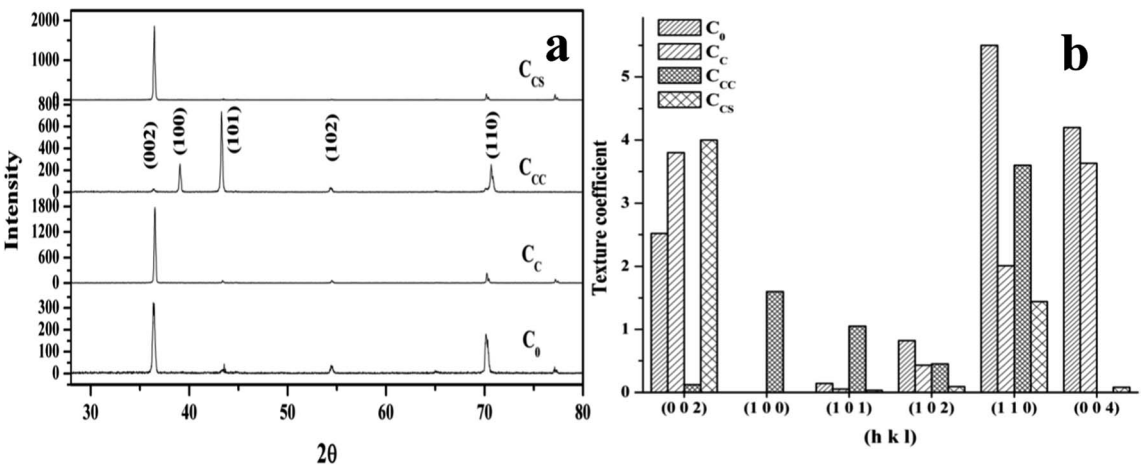

Fig. 3 (a) XRD and (b) texture coefficients for the zinc deposits.

$$Zn(OH)_{ads} + e^- \rightarrow Zn + OH^-$$

$$Zn(OH)_{ads} + (ZnOH)^+ + 2e^- \rightarrow Zn + OH^- + Zn(OH)_{ads}$$

It is seen from the cathodic polarization curves that the addition of HNTs to the electrolyte causes the reduction potential of zinc to shift towards larger negatives but the slope of the reduction curve remains unchanged. The shift to a lower value of reduction potential is attributed to a decrease in the active surface area of the cathode due to the adsorption of particles, and may also relate to the decrease in ionic transport by the HNTs, which does not significantly affect the electrochemical reaction mechanism. While comparing the effect of surfactants, CTAB, being a cationic surfactant, directs a higher number of particles towards the cathode compared to SLS, which is an anionic surfactant. Therefore, CTAB shifts zinc deposition to higher negative values.[17,20,21]

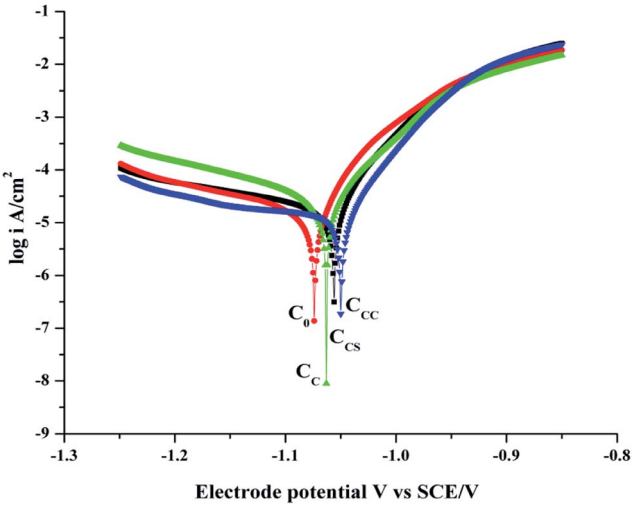

Fig. 5 Tafel curves for zinc films in 3.5 wt% NaCl solution.

3.4 Electrochemical studies

Tafel polarization study was conducted to calculate the kinetic parameters of the corrosion process. The plots were obtained by varying the potential of the deposits by ±200 mV from the open circuit potential at a scan rate of 0.01 V s^{-1} using 3.5% NaCl at 25 °C. The corrosion potentials (E_{corr}), corrosion rates (CR) and anodic/cathodic Tafel slopes (β_a and β_c) were obtained from the Tafel plots and are listed in Table 3. The polarization resistance values were determined using the relationship:[22]

$$I_{corr} = \frac{\beta}{R_p}$$

where β is a constant calculated by the following equation:

$$\beta = \frac{\beta_a \beta_c}{2.3(\beta_a + \beta_c)}$$

where β_a and β_c (V^{-1}) are the Tafel slopes and R_p (Ω cm^2) is the polarization resistance, and corrosion rates (CR) were calculated by the following equation

$$CR = \frac{0.13\ I_{corr}\ \text{Eq. Wt.}}{d}$$

where Eq. Wt is the equivalent weight and d is the density (g cm^{-3}) of the zinc metal.

The Tafel plots were registered for various zinc coatings, as shown in Fig. 5. It can be clearly noted that R_p values are higher for composites compared to the plain zinc coating. The composite coatings deposited in the presence of CTAB shows the highest R_p of 1001 Ω cm^2 and the least negative corrosion potential of −1.048 V; thus, the highest corrosion resistance compared to that obtained in the presence of SLS.

Electrochemical impedance spectroscopic measurements were also carried out to examine the chemical behavior of the zinc deposits. An equivalent circuit consisting of 2RC circuits shown in Fig. 6a was proposed. The two loops in the Nyquist diagram shown in Fig. 6b indicate that the process consists of two relaxations or two time constants. All the curves are of the same nature differing only in their point of intersection with Z_{real} axis, which is the quantitative characteristic of corrosion resistance. High frequency elements are related to the dielectric character C_{cot} of the coating that is reinforced by ionic conduction through its pores (R_{cot}). Further, low frequency contribution is attributed to the double layer capacitance (C_{dl}) at the coating electrolyte interface at the bottom of the pores coupled with the charge transfer resistance R_{ct}. The extent of chemical inertness for the selected corrosive medium can be analyzed through the resistance offered by the specimen, considering both the coating and charge transfer resistance values. The bare zinc, C_0 possesses 110.9 Ω. The introduction of particles to the zinc matrix increases corrosion resistance to 178.7 Ω. The presence of surfactants makes the composite more beneficial in terms of protection ability by enhancing the reinforcement. Higher corrosion resistance *i.e.*, 534.4 Ω in the presence of CTAB and 351.4 Ω with SLS advocates the above-mentioned discussion (Table 4). The total resistance ($R = R_{cot} + R_{ct}$) increases with the addition of HNT particles into the growing zinc matrix. The Bode plots are displayed in Fig. 6c. The

Table 3 Corrosion data for zinc coatings from Tafel experiments

Sample	E_{corr} V	PR Ω cm^2	I_{corr} A cm^2	CR g h^{-1}
C_0	−1.077	603	4.2×10^{-5}	8.7×10^{-5}
C_C	−1.061	679	3.2×10^{-5}	3.9×10^{-5}
C_{CC}	−1.048	1001	2×10^{-5}	2.7×10^{-5}
C_{CS}	−1.056	979	2.3×10^{-5}	2.8×10^{-5}

Table 4 Resistance values obtained from EIS experiments

Sample	$R = R_{cot} + R_{ct}$ Ω cm^2
C_0	111
C_C	179
C_{CS}	351
C_{CC}	534

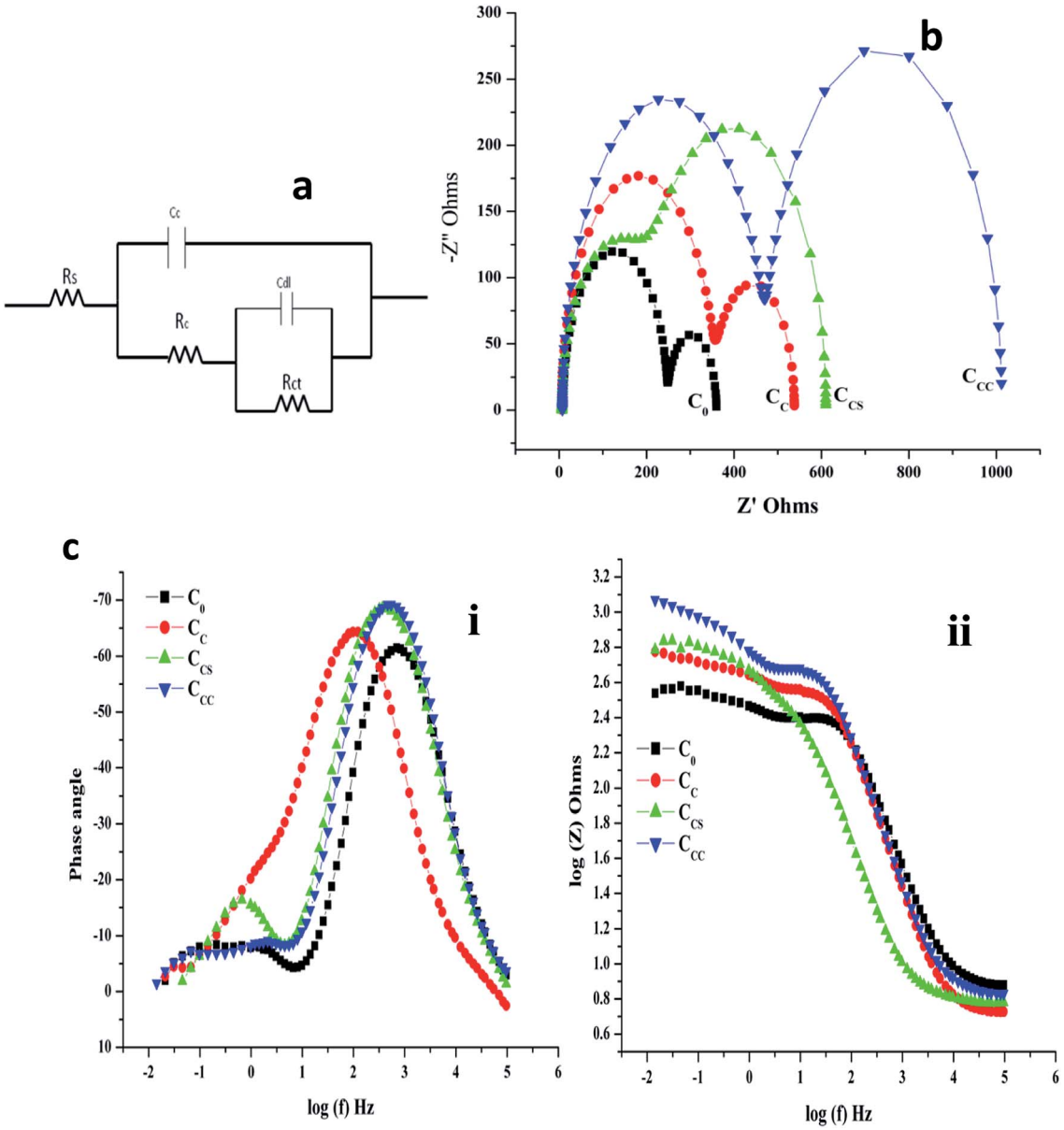

Fig. 6 (a) Equivalent circuit, (b) Nyquist plots for zinc deposits in 3.5 wt% NaCl solution and (c) Bode plots (i) phase angle *vs.* frequency (ii) impedance *vs.* frequency.

phase angle plot shows two humps, which reflect the two relaxation phenomena involved in the process. The impedance plot confirms the highest impedance value for the deposit C_{CC}. In addition, it is found that corrosion resistance is highest for the zinc composite deposited with CTAB. This can be seen by the fact that the particle incorporation of HNTs is increased by 4.8 wt%, whereas the composite with SLS can only increase particle incorporation of up to 4.1 wt%[23,24] In the absence of surfactants, the particle content was only 3.6 wt% in the deposit C_C. Halloysite nanotubes have been used as reinforcement to the growing zinc metal matrix, and the resulting composite coating exhibits superior electrochemical properties. This enhanced property is a major contribution of the secondary material introduced to the metal coating, and can be further enhanced by increasing the particles being incorporated. Factors governing particle incorporation include particle size and shape, relative density of the particles, inertness of the particles, concentration of the particles in plating bath, method and degree of adhesion, the orientation of the part being plated, *etc.* Some methods such as mechanical stirring/sonication and the usage of surfactants enhance particle deagglomeration and also lead to increased incorporation. The types of the second phase materials added to the coating are considerably diverse, consisting of different metal oxides, carbides and nitrides. These materials markedly improve the properties of the bare zinc. CNTs from the carbonaceous family being very strong and highly chemically inert have attracted the scientific interest; however, they are very expensive and their synthesis is very

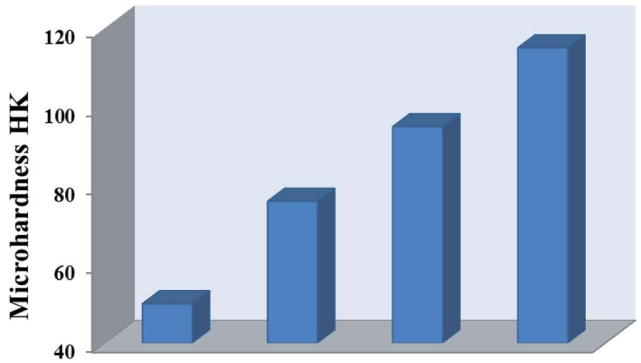

Fig. 7 Bar diagram showing the microhardness values for various zinc deposits.

tedious. HNTs are very similar to CNTs in terms of structure but are very cheap, readily available naturally and superior to CNTs because HNTs disperse better in solutions or polymer/metal matrices and never intertwine each other, unlike CNTs. This leads to significantly improved properties of their composites.[1,7,16,21,22]

The SEM image shows that the deposit C_{CC} has a smaller grain size, and the XRD results also support this argument. Here, it should be noted that particle distribution in the metal matrix plays crucial role, and clearly a more uniform distribution will lead to an improvement in surface properties. In this respect, surfactants are affected severely by adsorbing onto the particle surface. This is particularly true with CTAB because it not only adsorbs on the surface but also develops a positive surface charge that can accelerate its incorporation on the cathode. Similarly, CTAB promotes the even distribution of the particles in the composite compared to others. Further, as the particle content increases, the effective area exposed to the corrosive medium decreases and this may fill up any gaps, crevices or holes present in the growing metal matrix, leading to a compact and fine grained deposit.

3.5 Microhardness

The hardness of the coated panels are shown in the Fig. 7. The hardness of the deposits with the introduction of HNTs can be observed from the graph. The composite coating possesses higher hardness compared to plain zinc deposit. The deposits C_{CS} and C_{CC} are fine grained because of the presence of surfactants. In addition, the included particles were found to increase with the addition of surfactants. The composite prepared with CTAB exhibits the highest hardness because it contains high number of included HNTs. During hardness measurements, the dispersed particles in the fine grained matrix may obstruct easy dislocations that was shown by the higher hardness values of composite coatings fabricated in the presence of surfactants.[25]

4 Conclusion

Zinc and its HNT composite films were fabricated successfully. The incorporation of particles was confirmed by EDX technique. CTAB and SLS enhanced the incorporation of HNT in the deposit. Cathode polarization effect was appreciable in the presence of HNT, and rendered the composite more corrosion resistant. Higher particle incorporation and fine grained crystal structure made Zn–HNT composite better than bare coating. In addition, the microhardness of the deposit was influenced greatly by amount of incorporated particles. The composite that was fabricated in the presence of CTAB successfully incorporated a large number of particles and showed the highest hardness values.

Acknowledgements

The authors thank Kuvempu University Karnataka, India for providing lab facilities to bring about this work, and CSIR, Govt. of India for financial support by awarding Senior Research Fellowship (CSIR sanction no. 9/908(0003)2K12-EMR-I). Authors acknowledge the Indian Institute of Science, Bangalore for extending some experimental facilities and Dr Michael Rajamathi, Dept. of Chemistry, St. Joseph's College, Bangalore for providing the XRD facility.

References

1 B. M. Praveen, T. V. Venkatesha, Y. A. Naik and K. Prashantha, *Surf. Coat. Technol.*, 2007, **201**, 5836–5842.
2 S. Ranganatha, T. V. Venkatesha, K. Vathsala and M. K. Punith kumar, *Surf. Coat. Technol.*, 2012, **208**, 64–72.
3 S. Ranganatha, T. V. Venkatesha and K. Vathsala, *Mater. Res. Bull.*, 2012, **47**, 635–645.
4 S. Ranganatha, T. V. Venkatesha and K. Vathsala, *Ind. Eng. Chem. Res.*, 2012, **51**, 7932–7940.
5 S. Ranganatha and T. V. Venkatesha, *Ind. Eng. Chem. Res.*, 2013, **52**, 6422–6429.
6 S. Ranganatha, T. V. Venkatesha and K. Vathsala, *Appl. Surf. Sci.*, 2010, **256**, 7377–7383.
7 B. M. Praveen and T. V. Venkatesha, *J. Alloys Compd.*, 2009, **482**, 53–57.
8 N. Boshkov, *Surf. Coat. Technol.*, 2003, **172**, 217–221.
9 Z. F. Lodhia, J. M. C. Mol, W. J. Hamer, H. A. Terryn and J. H. W. De Wit, *Electrochim. Acta*, 2007, **52**, 5444–5452.
10 M. Liu, B. Guo, M. Du, X. Cai and D. Jia, *Nanotechnology*, 2007, **18**, 455703.
11 S. Ranganatha, T. V. Venkatesha and K. Vathsala, *Appl. Surf. Sci.*, 2012, **263**, 149–156.
12 H. Ismail, P. Pasbakhsh, M. N. Ahmad Fauzi and A. Abu Bakar, *Polym. Test.*, 2008, **27**, 841–850.
13 Y. Tang, S. Deng, L. Ye, C. Yang, Q. Yuan, J. Zhang and C. Zhao, *Composites, Part A*, 2011, **42**, 345–354.
14 R. Frost, *Clays Clay Miner.*, 1995, **43**, 191–195.
15 X. Sun, Y. Zhang, H. Shen and N. Jia, *Electrochim. Acta*, 2010, **56**, 700–705.
16 A. Gomes and M. I. da Silva Pereira, *Electrochim. Acta*, 2006, **51**, 1342–1350.
17 R. Sen, S. Bhattacharya, S. Das and K. das, *J. Alloys Compd.*, 2010, **489**, 650–656.

18 M. Rezrazi, M. L. Dochi, P. Bercot and J. Y. Hihn, *Surf. Coat. Technol.*, 2005, **192**, 124–130.
19 B. M. Praveen and T. V. Venakatesha, *Appl. Surf. Sci.*, 2008, **254**, 2418–2424.
20 K. O. Nayana and T. V. Venkatesha, *J. Electroanal. Chem*, 2011, **663**, 98.
21 J. Fustes, A. Gomes and M. I. da Silva Pereira, *J. Solid State Electrochem.*, 2008, **12**, 1435–1443.
22 K. Vathsala and T. V. Venakatesha, *J. Solid State Electrochem.*, 2012, **16**, 993–1001.
23 C. Guo, Y. Zuo, X. Zhao, J. Zhao and J. Xiong, *Surf. Coat. Technol.*, 2008, **202**, 3385–3390.
24 L. Shi, C. F. Sun, P. Gao, F. Zhou and W. M. Liu, *Surf. Coat. Technol.*, 2006, **200**, 4870–4875.
25 B. M. Praveen and T. V. Venkatesha, *Appl. Surf. Sci.*, 2008, **254**, 2418–2424.